X-ray imaging microscope with a partial coherent illumination

Akihisa Takeuchi*, Hidekazu Takano, Kentaro Uesugi and Yoshio Suzuki
JASRI / SPring-8, Kouto 1-1-1, Mikazuki-Tyo, Sayo-Gun, Hyogo 679-5198, Japan

ABSTRACT

An x-ray imaging microscopy experiment was performed at the x-ray energy of 8 keV. A Fresnel zone plate (FZP) fabricated by electron-beam lithography technique was used as an objective. Material of the zone structure is tantalum. The experiment was done at the undulator beamline BL47XU of SPring-8. Undulator radiation was monochromatized by passing through a liquid nitrogen cooled Si 111 double crystal monochromator. In order to eliminate speckle-like background noise, a partial coherent illumination was introduced by using a "beam diffuser" consisted of graphite powder. Beam spread of the illumination with the diffuser was about 35 μrad. A charge coupled device (CCD) camera coupled with a phosphor screen and a microscope objective (x 12 or x 24) was used as an image detector. Converted pixel size with the x 24 lens was 0.5 μm. Magnification of the x-ray microscope system was set to be 7.61 - 13. Pitch of 0.6 μm (0.3 μm line and 0.3 μm space) pattern of the test chart was resolved, and the outermost zone structure of the same type of FZP was observed. Imaging properties are also discussed by using Hopkins' optical imaging theory.

Keywords: X-ray microscopy, Fresnel zone plate, synchrotron radiation, partial coherent illumination

1. INTRODUCTION

Although it takes only about 10 years or less since the developments of hard x-ray micro-imaging have been started, spatial resolution has been already achieved sub-μm order and is now getting ahead of that of the visible light microscopy. Various types of hard x-ray optical devices have been developed mainly as focusing devices for generating x-ray microbeams. However, some types of them are started developing also as microscope objectives, e.g.; Fresnel zone plate (FZP)[1-3], Bragg-Fresnel optics (BFO)[4], refractive lenses[5, 6] and Wolter type mirror[7 - 10]. Also imaging microscope systems using these objectives have achieved μm order or sub-μm resolution.

Advent of the 3rd generation synchrotron radiation (SR) light source which supplies high flux density beam enables to design high-magnification and high-resolution x-ray microscope system. However, another property of SR source, highly-coherent beam, is unwelcome for the illumination of the imaging microscope. It is because images and backgrounds tend to be modulated by interference between the incident beam and the diffracted beam when highly-coherent beam is used for illumination. Moreover, if surface errors of the optical devices such as windows, monochromator, and objective are not sufficiently small, images are deteriorated by speckle-like noise[11-14]. That is why the coherence as low as possible is proper for the illumination of the imaging microscope. Kagoshima et. al. performed incoherent illumination imaging at x-ray energy of 10 keV by scanning a condenser two-dimensionally during exposure[3]. They also succeeded in widening the field of view with this method. However, because the original field of view illuminated by condenser is small, this method needs a long exposure time for condenser scanning even if the photon flux is enough high. White et. al. showed a partial coherent illumination imaging in soft x-ray region by using a beam diffuser plate. In order to average out the effect of speckle caused by the diffuser plate itself, it was moved during exposure[15]. In the hard x-ray region, Awaji et. al. used this method at 25 keV[16]. This method enables to use incident beam from the SR source directly. Hence not so long exposure time is needed if the transmittance of the diffuser is high. However, especially in the hard x-ray region, due to the lack of materials with large scattering angle, it is difficult to produce perfect incoherent illumination. Therefore the illumination is always obliged to be the partial coherent, however, which must be difficult in order to evaluate the precise imaging properties.

Recently we have developed a hard x-ray imaging microscope system with SR source, FZP objective and beam diffuser for partial coherence illumination. In this paper, we describe the estimation of imaging properties of this system using Hopkins' theory, and compare the estimation with the experimental data.

*Correspondence: E-mail: take@spring8.or.jp; Telephone: +81-791-58-0833; Fax: +81-791-58-0830

2. EXPERIMENTAL SETUP

A schematic diagram of the experimental setup is shown in Figure 1. The experiment was carried out at the R & D beamline BL47XU of SPring-8. The system consists of a light source (undulator installed storage ring of SPring-8), double crystal monochromator, a beam diffuser, pinholes, a Fresnel zone plate objective, and an image detector.

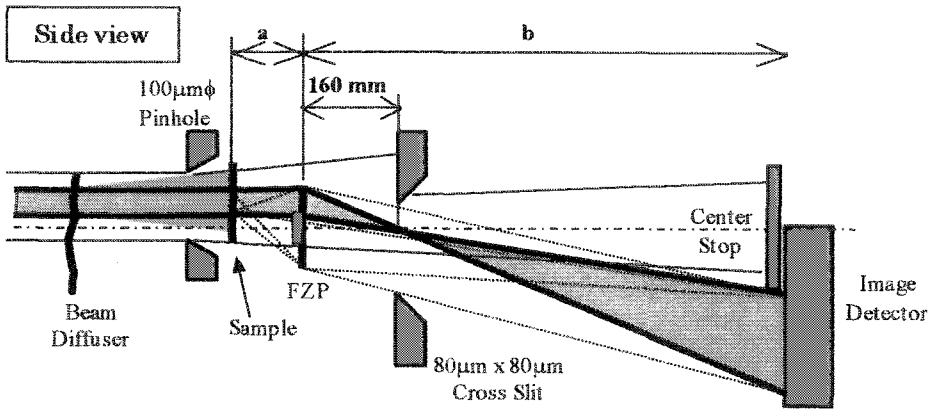

Figure 1. Schematic diagram of the experimental setup. FZP: Fresnel zone plate. Magnification was set to be from x 7.61 (a = 181 mm and b = 1379 mm) to x 13 (a = 172.3 mm and b = 2240mm).

"In vacuum type" 139 pole undulator radiation was used as a light source. X-ray energy was chosen to be 8 keV by passing through a lq-N_2 cooled type Si 111 double crystal monochromator.

The vertical spatial coherence at the experimental hutch of this beamline was measured to be about 80 μm at the X-ray energy of 8 keV. In this case the angular deviation of the incident beam was about 1 – 2 μrad. As mentioned in previous chapter, illumination using such a highly-coherent beam deteriorates image properties. Therefore in order to decrease the coherence, a beam diffuser (graphite powder; grinded by mortar and pasted on a thin film) was installed just in front of the sample, and was rotated during the acquisition of the images to shade off the speckle-like noise from the diffuser itself[15]. Using this, the angular spread of illumination at the sample was about 35 μrad in full width at half maximum (FWHM) as shown in Figure 2. Transmittance was about 50 %.

A Fresnel zone plate (FZP) was used as a microscope objective. SEM image of the FZP is shown in Figure 3. This was fabricated by using electron-beam lithography technique at NTT-AT (Nippon Telephone and Telegram Advanced

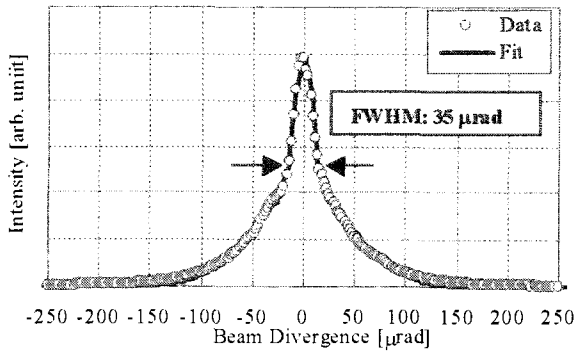

Figure 2. Intensity distribution of the incident beam with the beam diffuser (graphite powder), circled dot: measured data, solid line: fitted by two gaussians.

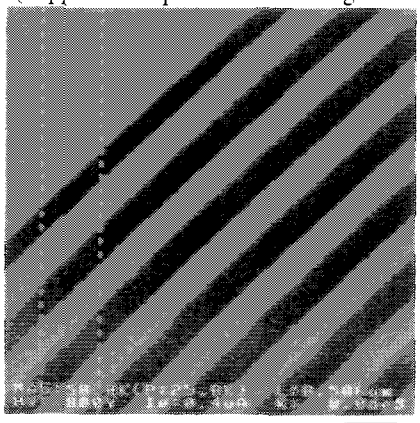

Figure 3. SEM image of around the outermost zone of the objective Fresnel zone plate.

Technology). The zone structure with outermost zone width of 0.25 μm was made of 1 μm-thick tantalum. The diameter of FZP is 100 μm, number of zone is 100, and the focal length of the 1st order is 160 mm at the X-ray energy of 8 keV. A center beam stop (2 μm-thick gold) with diameter of 50 μm is deposited on the FZP. With the microbeam knife-edge scan test of the FZP, a focal spot size was measured to be 0.3 μm in FWHM which was almost equal to the diffraction limit[17]. In order to select only the first-order diffraction of the FZP, a pinhole (100 μm in diameter), cross slits (opening size: 80 μm x 80 μm), and a center beam stop (gold wire: 200 μm in diameter) were installed in front of the sample, at the back focal plane and in front of the detector, respectively. And from the same reason, more than half of the field of view was blind by the center stop. Therefore the system is off-axis configuration in the vertical direction as shown in Figure 1. Optical axis was shifted about 30 - 40 μm from the center of the FZP in the vertical direction.

The image detector consists of a single crystal phosphor screen (Lu_2SiO_5: Ce, <10 μm in thickness), a microscope objective (x 12 or x 24) and a cooled charge coupled device (CCD) camera (Figure 4(a), Hamamatsu Photonics K. K., Japan). Pixel size of the CCD camera is 12 μm x 12 μm and number of pixel is 1000 (H) x 1018 (V). Therefore the converted pixel size of the detector system is 1 μm x 1 μm or 0.5 μm x 0.5 μm. The point spread functions of the detector with both microscope objectives are measured, and in each case FWHM is found to be about 2 pixels[18]. Modulation transfer function (MTF) of the detector obtained from the Fourier transform of the point spread function data is shown in Figure 4(b).

Magnification of the X-ray microscope system was set to be 7.61 – 13. A tantalum test chart (0.5 μm thickness) was used as a sample. It was designed for evaluation of the imaging properties such as the spatial resolution and MTF. It was also fabricated by using the electron-beam lithography technique at NTT-AT.

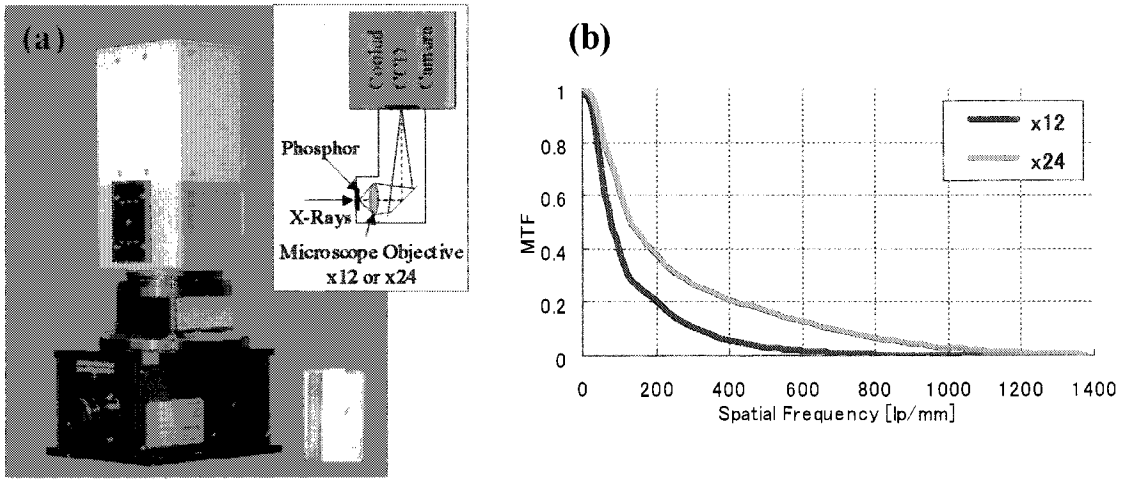

Figure 4. Image detector "Beam Monitor AA50" (Hamamatsu Photonics K.K., Japan). (a) photograph and schematic drawing of the optical system. (b) Modulation transfer function (MTF) obtained from the measured point spread function data, (black line; microscope objective of x12, gray line; of x24)[17].

3. IMAGING PROPERTIES OF PARTIAL COHERENT ILLUMINATION SYSTEM

In order to estimate the imaging properties of this experimental setup, it is necessary to consider the effect of the partial coherent illumination because the graphite beam diffuser cannot supply incoherent illumination. The MTF for the partial coherent illumination is calculated with supposing the object has a periodic transmittance distribution like a sine wave. For simplify, let us consider only one direction of the imaging properties.

From Hopkins' optical imaging theory, one-dimensional intensity distribution of the image with partial coherent illumination microscope system is expressed as following equation with omitting constant[19].

$$I(x) = \iint_{-\infty}^{\infty} C(s;s')T(s)T^{*}(s')\exp[2\pi i(s-s')x]dsds' \quad , \qquad (1)$$

where $T(s)$ is a Fourier transform of the amplitude transmittance of the object. $C(s;s')$ is a transmission cross-coefficient of the system, expressed as

$$C(s;s') = \iint_{-\infty}^{\infty} \left|P_2(u,v)\right|^2 P_1(\tilde{s}+u,v)P_1^*(\tilde{s}'+u,v)dudv \quad , \tag{2}$$

where $\tilde{s} = s\lambda f_1$, $\tilde{s}' = s'\lambda f_1$, f_1 is the focal length of the objective. $P_1(u,v)$ is the pupil function of the objective, and $P_2(u,v)$ is the effective source or the pupil function of the condenser.

In this estimation, let us assume that the amplitude transmittance of the object is approximated as one-dimensional cosine wave function given as

$$t(x) = \frac{1}{2}\{1 + a\cos(2\pi sx)\} \quad , \tag{3}$$

where a is assumed as real number supposing the object is an absorbing material.

In the case of the on-focus imaging, $P_1(u,v)$ is real number. Therefore from Eqs. (1) - (3), we get

$$I(x) = \frac{1}{4}\{1 + 2aC(s;0)\cos(2\pi sx) + \frac{1}{2}a^2C(s;s) + \frac{1}{2}a^2C(s;-s)\cos(4\pi sx)\} \quad , \tag{4}$$

On the other hand from Eq. (3), intensity transmittance of the object is

$$O(x) = \left|t(x)\right|^2 = \frac{1}{4}\{1 + 2a\cos(2\pi sx) + \frac{1}{2}a^2 + \frac{1}{2}a^2\cos(4\pi sx)\} \tag{5}$$

Therefore the MTF can be represented as the frequency response function comparing Eq. (4) and Eq. (5),

$$\begin{aligned} R(s) &= \frac{(I_{\max} - O_{\min}) - (I_{\min} - O_{\min})}{(I_{\max} - O_{\min}) + (I_{\min} - O_{\min})} = \frac{I(1/s) - I(1/2s)}{I(1/s) + I(1/2s) + 2O(1/2s)} \\ &= \frac{C(s;0)}{1 + \frac{a}{4}(C(s;s) + C(s;-s) - 2)} \end{aligned} \tag{6}$$

If the absorption of the object is small ($a << 1$), we can consider $R(s) \approx C(s;0)$. This approximation can be normally applied for fine structures near the diffraction limit.

Using Eq. (6), MTF of the FZP under the same condition with the experimental setup is calculated. In the calculation, the pupil function of the objective $P_1(u,v)$ is set as

$$P_1(u,v) = \begin{cases} 1 & \varepsilon_1 r_1 \le \sqrt{(u-u_d)^2 + (v-v_d)^2} \le r_1, \\ 0 & elsewhere, \end{cases}$$

where r_1 is the radius of the objective and ε_1 is the obstruction ratio of the objective. u_d and v_d are the off-axis distance of horizontal direction and of vertical direction, respectively. In this case, r_1 = 50 [μm], ε_1 = 0.5, and off-axis parameters are u_d = 0 and v_d = 37.5 [μm] (the pupil is shifted 3/4 times of the radius of objective in the vertical direction). Therefore the horizontal direction corresponds to the normal to the off-axis direction, and the vertical direction corresponds to the parallel to it. As the effective source $P_2(u,v)$, profile of the beam divergence distribution fitted with two Gaussians shown in Figure 2 is used. The reason why fitting curve is used is in order to decrease the noise in the high frequency region. Two-dimensional maps of $P_1(u,v)$ and $P_2(u,v)$ are shown in Figure 5(a) and Figure 5(b), respectively. Figure 6 shows calculated

MTFs with these parameters. For comparison, MTFs of both coherent illumination and incoherent illumination are also shown. Because of the off-axis system, imaging properties are different between vertical direction and horizontal direction. Hence MTF in each direction is shown independently.

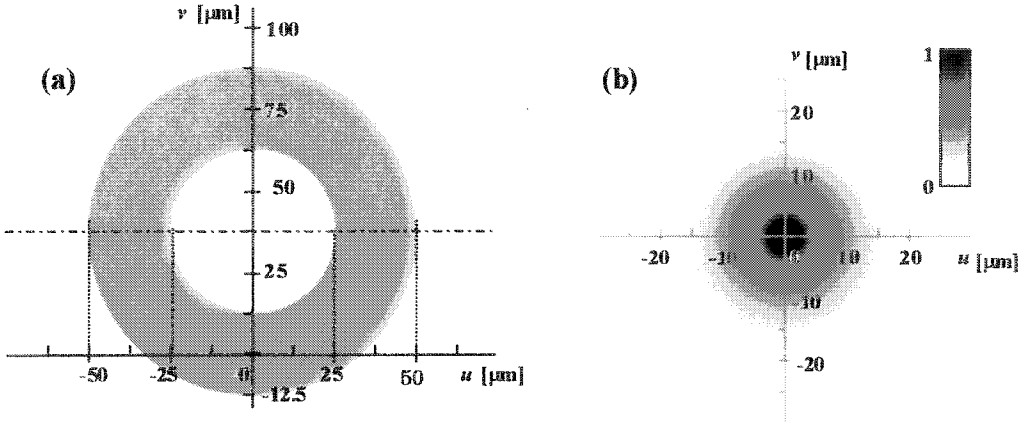

Figure 5. Two-dimensional mapping of the pupil function. (a) Pupil function of the objective FZP $P_1(u,v)$, (b) Effective source function of the illumination with graphite beam diffuser $P_2(u,v)$.

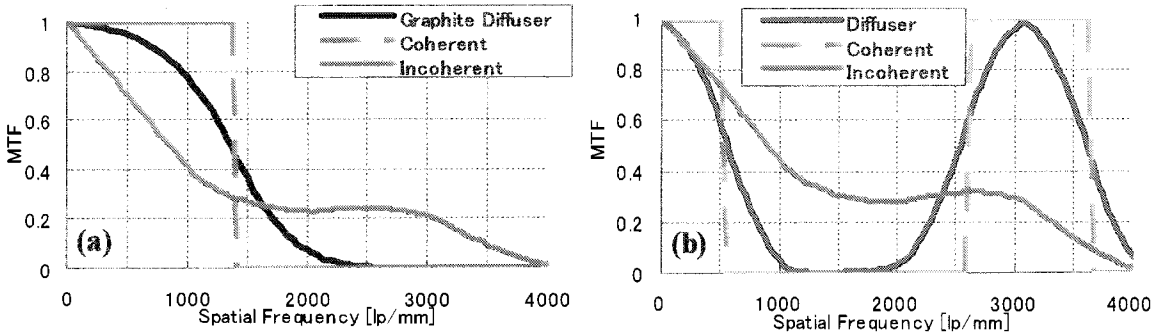

Figure 6. Modulation transfer function (MTF) of the objective FZP for coherent illumination (broken gray), incoherent illumination (solid gray), and illumination with graphite beam diffuser (solid black). (a) in horizontal direction, (b) in vertical direction.

Schematic drawing of the effective domain of integration for the transmission cross-coefficient $C(s;0)$ (Eq. (2)) is shown in Figure 7. The effective domain of integration is determined with the common area between the effective source (P_2), the pupil functions of FZP (P_1) shifted by $s\lambda f_1$, and the complex conjugate of P_1 (P_1^*) shifted by $s'\lambda f_1$ (here, $P_1 = P_1^*$, and $s' = 0$), as shown shaded in the figure. In order to calculate the horizontal MTF, P_1 is shifted along u-axis (Figure 7(a)). And in the case of the vertical MTF, P_1 is shifted along v-axis (Figure 7(b)).

As the horizontal MTF, if the radius of P_2 is small (coherence is high) such as the illumination with the graphite diffuser, as shown in Figure 7(a) P_2 does not overlap the obstructed area of P_1. Hence as shown in Figure 6(a), the frequency response becomes monotonously smaller as the spatial frequency becomes higher, without response enhancing in the higher frequency region typically seen in the annular aperture system (see MTF of incoherent illumination in Figure 6). The response becomes zero at the spatial frequency of 2500 line pair / mm. This value corresponds to the spatial resolution of 0.4 μm, which is not achieved at the diffraction limit of the objective (0.3 μm). It is because the diameter of P_1 does not fully used due to the off-axis configuration and due to small P_2. Therefore large P_2 (lower coherence) is preferable for high resolution.

On the other hand, as the vertical direction, it is evident from Figure 7(b) that the obstructed area of P_1 must pass through P_2. Therefore as shown in Figure 6(b), response peak exists in the high frequency region and becomes more conspicuous as the coherence becomes higher. In the case of the illumination with diffuser, response peak with almost 100 % is separated to

lower frequency region (up to 1000 lp /mm) and higher frequency region (2000 – 4000 lp /mm). And there is almost no response in the middle region of 1000 - 2000 lp /mm. Therefore the spatial resolution achieves 0.25 μm, however, the structures of 0.5 – 1 μm pitch cannot be resolved. It is evident that it is due to the effect of the annular aperture of the objective. If the radius of P_2 is smaller than that of obstructed area of P_1, non-response area exists in the middle frequency region like this case.

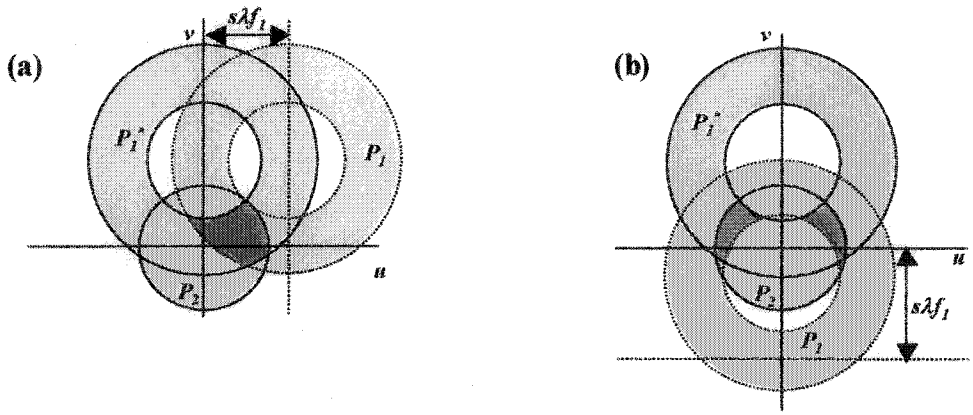

Figure 7. Schematic drawing of the effective domain of integration (shown shaded) for the transmission cross-coefficient $C(s;0)$ for the off-axis imaging system with an annular pupil objective. (a) horizontal MTF (normal to the off-axis direction), (b) vertical MTF (parallel to the off-axis direction). P_1; pupil function of objective, P_2; effective source function.

4. RESULTS

4.1 Comparison with coherent illumination

In order to compare the coherent illumination and the partial coherent illumination with beam diffuser, a spoke patterned tantalum test chart was used as the object. Figure 8(a) shows the x-ray image obtained without beam diffuser (in this condition the coherence of the illumination was not actually perfect). Exposure time was 50 sec. Center of the shown area correspond to be at about 30 μm away in vertical direction from the objective axis. In this beamline, surfaces of optical devices such as monochromator and Be windows are carefully polished, and the objective FZP was fabricated in good condition. Therefore typical speckle-like noise was not seen. However, it can be clearly seen that the background was deteriorated and the image was modulated by interference pattern. This phenomenon is more typically in the vertical direction because the coherence is higher in this direction. Figure 8(b) represents the x-ray image of the same object obtained with the graphite beam diffuser. Exposure time was 100 sec. The background noise and the modulation of the image decrease evidently due to the decline of the coherence. However, because the coherence still remains in the illumination, the effect of the edge-enhance is still seen.

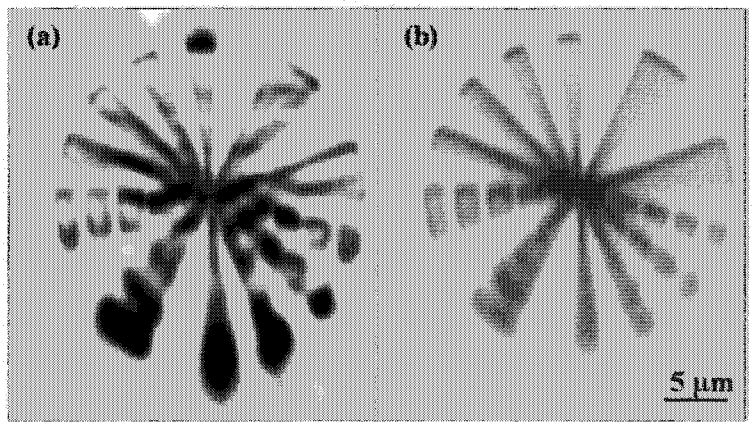

Figure 8. X-ray image of a spoke test pattern (Ta; 0.5 μm thickness), (a) coherent illumination, (b) partial coherent illumination (with graphite beam diffuser).

4.2 Estimation of the MTF

For comparison with the calculated value of the MTF as shown in Figure 6, experimental value of the MTF is measured using a tantalum test chart with periodical patterns as the sample. As shown in Figure 9(a), this sample consists of rectangular periodical patterns with various pitches from 0.1 μm (10000 lp /mm). Therefore by measuring the image contrast of each pitch pattern, experimental value of MTF can be plotted. X-ray image obtained with this system is shown in Figure 9(b). Exposure time was 100 sec. As shown in this figure, image properties are different between the vertical direction and the horizontal direction. As the horizontal direction, images of up to 0.6 μm pitch were resolved. As the vertical direction, although 0.4 μm pitch patterns were resolved, 0.6 μm – 1.0 μm pitch patterns were not. Figure 10(a) and (b) represent the intensity profile obtained from the x-ray images of the test chart. And Figure 10(c) and (d) show the experimental value of MTF (plot) measured from the profile data (a) and (b), respectively. In each graph, solid line represents the calculated MTF using Eq.

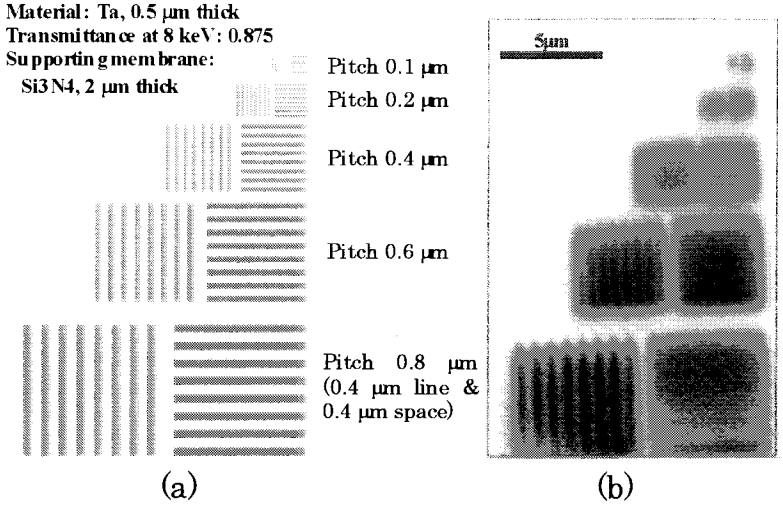

Figure 9. Ta test chart for MTF measurement. (a) schematic drawing and parameters, (b) X-ray image.

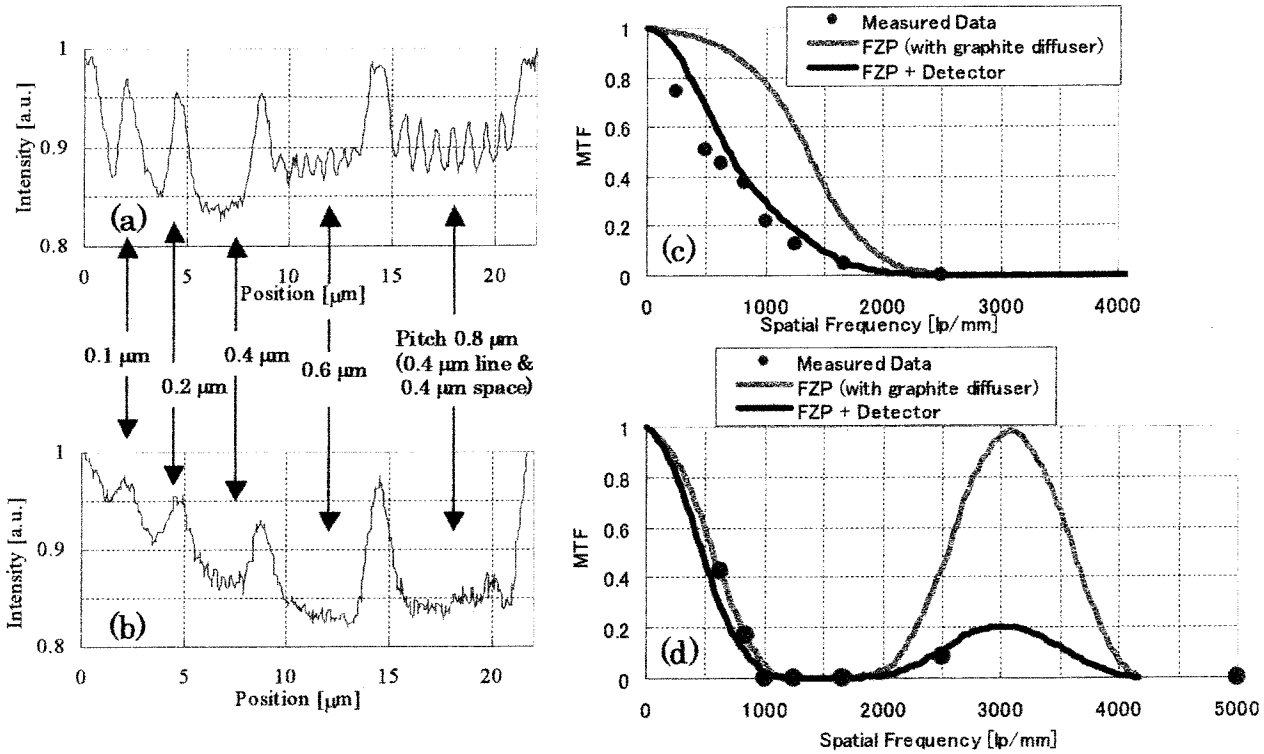

Figure 10. Intensity profile of the X-ray image of rectangular periodic test pattern shown in Figure 9, (a) in horizontal direction, and (b) in vertical direction. (c), (d) MTF obtained from the profile data (a) and (b), respectively.

(6), and including additional consideration such as

$$R'(s) = R(s)R_D(s/M),$$

where $R(s)$ is the MTF calculated from Eq. (6) (represented by gray line in Figure 10(c), (d)), $R_D(s)$ is the MTF of the detector (Figure 4(b)), and M is the magnification ratio of the x-ray microscope system. It is evident that the calculated value of MTF has a good agreement to the measured value in each direction. As the spatial frequency is higher, the response becomes more deteriorated by the detector. Hence in the vertical MTF the response peak in the higher frequency decreases extremely. In order to increase the response in the higher frequency region, magnification should be larger. As shown in Figure 6, it is necessary much lower coherent illumination to lessen the difference of imaging properties between the horizontal direction and the vertical direction: to achieve the horizontal spatial resolution to the diffraction limit, and to increase the response of middle frequency range in the vertical direction.

Figure 11(a) shows a calculated MTF in the case of the pupil function is shifted 3/4 times of the radius in both horizontal and vertical directions from the axis. This corresponds to the MTF for an object with 45 degree inclined structure. This MTF gives a good response in the middle frequency range due to the influence of the horizontal MTF (Figure 10(c)), and also in the higher frequency range good response remains due to the influence of the vertical MTF (Figure 10(d)). Figure 11(b) shows an x-ray image of a FZP whose parameters are same as the objective. Center of the shown area correspond to be at about 30 μm away from the objective axis in both directions. All of the zone structure from inner (~0.5 μm width; ~1.0 μm pitch) to outermost (0.25 μm width; ~0.5 μm pitch) can be observed that is impossible for only the vertical MTF or for only the horizontal MTF.

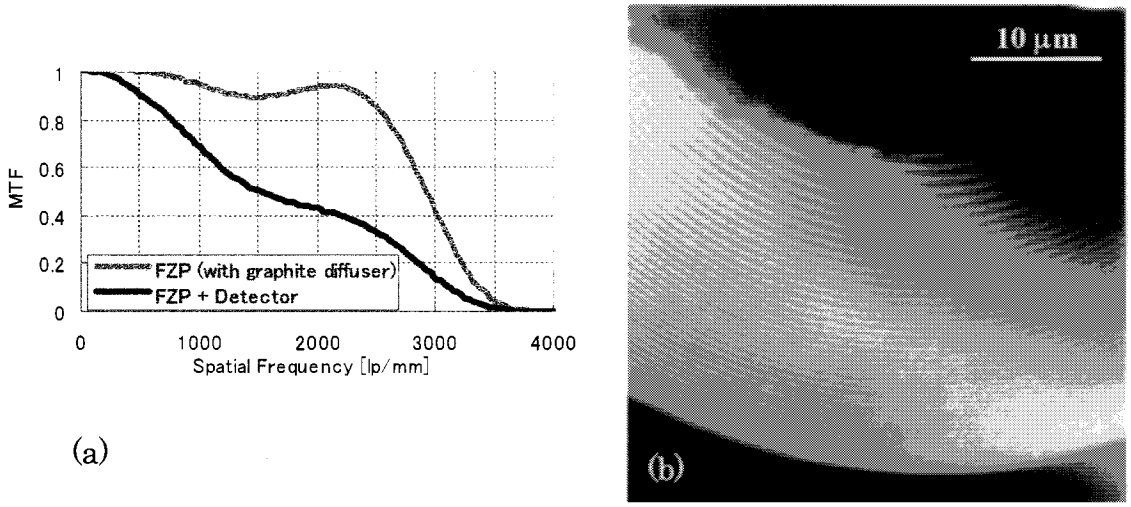

Figure 11. (a) Calculated MTF in the case of the objective pupil function is shifted 3/4 times of the radius in both direction. (b) X-ray image of a FZP, whose parameters are same as that of the objective FZP. Center of the shown area is located at same off-axis distance between horizontal direction and vertical direction.

REFERENCES

1. B. Lai, W. Yun, Y. Xiao, L. Yang, D. Legnini, Z. Cai, A. Krasnoperova, F. Cerrina, E. DiFabrizio, L. Grella and M. Gentili, "Development of a hard x-ray imaging microscope," Rev. Sci. Instrum. **66** (1995) No. 2, 2287.
2. M. Awaji, Y. Suzuki, A. Takeuchi, N. Kamijo, S. Tamura, M. Yasumoto and Y. Kohmura, "Imaging Hard X-Ray Microscopy with a Multilayer Fresnel Zone Plate," *Proc. VIth Int. Conf. X-Ray Microscopy, Berkeley, California*, 1999 (American Inst. Phys., 2000) p.545.
3. Y. Kagoshima, T. Ibuki, K. Takai, Y. Yokoyama, N. Miyamoto, Y. Tsusaka and J. Matsui, "500-nm-Resolution 10keV X-Ray Imaging Transmission Microscope with Tantalum Phase Zone Plate," Jpn. J. Appl. Phys. **39** (2000) 433.
4. A. Snigirev, I. Snigireva, P. Boeske, S. Lequien and I. Schelokov, "High energy X-ray phase contrast microscopy using a circular Bragg-Fresnel lens," Opt. Commun. **135** (1997) 378.

5. Y. Kohmura, M. Awaji, Y. Suzuki, T. Ishikawa, Y. I. Dudchik, N. N. Kolchevsky and F. F. Komarov, "X-ray focusing test and x-ray imaging test by a microcapillary x-ray lens at an undulator beamline," Rev. Sci. Instrum. **70** (1999) No. 11, 4161.
6. B. Lengeler, C. Schroer, J. Tümmler, B. Benner, M. Richwin, A. Snigirev, I. Snigireva and M. Drakopoulos, "Imaging by parabolic refractive lenses in the hard x-ray range," J. Synchrotron Rad. **6** (1999) 1153.
7. S. Aoki, "Axisymmetric Grazing Incidence Optics for an X-Ray Microscope and Microprobe," *X-ray Microscopy II*, ed. D. Sayre, M. Howells, J. Kirz and H. Rarback, (Springer Series in Optical Sciences, Springer-Verlag, Berlin, 1987), p. 102.
8. J. H. Underwood, A. C. Thomson, Y. Wu and R. D. Giauque, "X-ray microprobe using multiplayer mirrors," Appl. Opt. **25** (1986) No. 11, 1730.
9. A. Takeuchi, S. Aoki, K. Yamamoto, H. Takano, N. Watanabe and M. Ando, "Full-field x-ray fluorescence imaging microscope with a Wolter mirror," Rev. Sci. Instrum. **71** (2000) No. 3, 1279.
10. A. Takeuchi, K. Uesugi. Y. Suzuki and S. Aoki, "Hard X-Ray Microtomography Using X-Ray Imaging Optics ," Jpn. J. Appl. Phys. **40** (2001) 1499.
11. A. Snigirev, I. Snigireva, V. G. Kohn and S. M. Kuznetsov, "On the requirements to the instrumentation for the new generation of the synchrotron radiation sources. Beryllium windows," Nucl. Instrum. Methods A **370** (1996) 634.
12. A. Souvorov, I. Snigireva and A. Snigirev, "MIRROR SURFACE CHARACTERIZATION BY TOPOGRAPHY WITH COHERENT X-RAYS," *Proc.* SPIE **3113** (1997) 476.
13. Y.Suzuki, A.Momose and H.Sugiyama, "Characterization of windows and filters for coherent X-ray beamlines" J. Synchrotron Rad. **5** (1998) 596.
14. N. Watanabe, S. Aoki, H. Takano, K. Yamamoto, A. Takeuchi, H. Tsubaki and T. Aota, "Phase-Contrast Hard X-Ray Imaging Microscope with Wolter Mirror Optics," *Proc. VIth Int. Conf. X-Ray Microscopy, Berkeley*, California, 1999 (American Inst. Phys., 2000) p.84.
15. D. L. White, O. R. Wood II, J. E. Bjorkholm, S. Spector, A. A. MacDowell and B. LaFontaine, "Modulation of the coherence of undulator radiation," Rev. Sci. Instrum. **66** (1995) 1930.
16. M. Awaji, Y. Suzuki, A. Takeuchi, H. Takano, N. Kamijo, S. Tamura and M. Yasumoto, "X-ray imaging microscopy at 25 keV with Fresnel zone plate optics", to be published in Nucl. Instrum. Meths. A, *Proc. 7th Int. Conf. Synchrotron Radiation Instrumentation* (2000).
17. Y. Suzuki, A. Takeuchi, H. Takano, T. Ohigashi and H. Takenaka, "Diffraction-Limited Microbeam with Fresnel Zone Plate Optics in Hard X-Ray Regions," Jpn. J. Appl. Phys. **40** (2001) 1508.
18. H. Takano, Y. Suzuki, K. Uesugi, A. Takeuchi and N. Yagi, "Point spread function measurement of imaging detectors with an x-ray microbeam," to be published in *Proc.* SPIE (2001).
19. H. H. Hopkins, "On the diffraction theory of optical images," *Proc.* R. Soc. A **217** (1953) 408.